

UNCLASSIFIED

AD NUMBER

AD039949

CLASSIFICATION CHANGES

TO: unclassified

FROM: confidential

LIMITATION CHANGES

TO:

Approved for public release, distribution unlimited

FROM:

Distribution authorized to U.S. Gov't. agencies and their contractors; Administrative/Operational Use; Mar 1954. Other requests shall be referred to Wright Air Development Center, Wright-Patterson AFB, OH 45433.

AUTHORITY

Auth listed in ASTIA TAB no. U62-2-2 dtd 15 Apr 1962; Air Force Avionics Lab ltr, 17 Aug 1979

THIS PAGE IS UNCLASSIFIED

UNCLASSIFIED

AD 39 949

*Reproduced
by the*

**ARMED SERVICES TECHNICAL INFORMATION AGENCY
ARLINGTON HALL STATION
ARLINGTON 12, VIRGINIA**



**CLASSIFICATION CHANGED
TO UNCLASSIFIED
FROM CONFIDENTIAL
PER AUTHORITY LISTED IN
ASTIA TAB NO. 462-2-2
DATE 15 APR. 62**

UNCLASSIFIED

NOTICE: When government or other drawings, specifications or other data are used for any purpose other than in connection with a definitely related government procurement operation, the U. S. Government thereby incurs no responsibility, nor any obligation whatsoever; and the fact that the Government may have formulated, furnished, or in any way supplied the said drawings, specifications, or other data is not to be regarded by implication or otherwise as in any manner licensing the holder or any other person or corporation, or conveying any rights or permission to manufacture, use or sell any patented invention that may in any way be related thereto.

**NOTICE: THIS DOCUMENT CONTAINS INFORMATION AFFECTING THE
NATIONAL DEFENSE OF THE UNITED STATES WITHIN THE MEANING
OF THE ESPIONAGE LAWS, TITLE 18, U.S.C., SECTIONS 793 and 794.
THE TRANSMISSION OR THE REVELATION OF ITS CONTENTS IN
ANY MANNER TO AN UNAUTHORIZED PERSON IS PROHIBITED BY LAW.**

CONFIDENTIAL

WADC TECHNICAL REPORT 54-53

AD No. 39947
ASTIA FILE COPY

(TID: -- UNCLASSIFIED)
**SUBSONIC FLUTTER TESTS OF AN UNSWEPT
ALL-MOVABLE HORIZONTAL TAIL**

*NILES R. HOFFMAN
IRVIN N. SPIELBERG*

AIRCRAFT LABORATORY

MARCH 1954

WRIGHT AIR DEVELOPMENT CENTER

CONFIDENTIAL

54A A

56199

NOTICES

When Government drawings, specifications, or other data are used for any purpose other than in connection with a definitely related Government procurement operation, the United States Government thereby incurs no responsibility nor any obligation whatsoever; and the fact that the Government may have formulated, furnished, or in any way supplied the said drawings, specifications, or other data, is not to be regarded by implication or otherwise as in any manner licensing the holder or any other person or corporation, or conveying any rights or permission to manufacture, use, or sell any patented invention that may in any way be related thereto.

This document contains information affecting the National defense of the United States within the meaning of the Espionage Laws, Title 18, U.S.C., Sections 793 and 794. Its transmission or the revelation of its contents in any manner to an unauthorized person is prohibited by law.

CONFIDENTIAL

WADC TECHNICAL REPORT 54-53

(Title--UNCLASSIFIED)
**SUBSONIC FLUTTER TESTS OF AN UNSWEPT
ALL-MOVABLE HORIZONTAL TAIL**

*Niles R. Hoffman
Irvin N. Spielberg*

Aircraft Laboratory

March 1954

RDO No. 459-36T

Wright Air Development Center
Air Research And Development Command
United States Air Force
Wright-Patterson Air Force Base, Ohio

CONFIDENTIAL

54AA

56199

CONFIDENTIAL

FOREWORD

This project was carried out by the Dynamics Branch of the Aircraft Laboratory, Directorate of Laboratories, WADC, under Research and Development Order No. 459-36T, "Investigation of Flutter Problems of All-Movable Tails". The tests were conducted in the Wright Air Development Center Five Foot Wind Tunnel during February 1953. The authors were also the project engineers.

Mr. Leon A. Tolve materially assisted the work by many helpful suggestions. Mr. Francis F. Hense constructed the flutter model.

This report reveals information relating to flutter research and has applications to military aircraft design. Since the safeguarding of this information is necessary in the interests of national security, this report has been classified "Confidential" in accordance with paragraphs 2.s and 24.a. (9) of AFR 205-1.

WADC TR 54-53

CONFIDENTIAL

CONFIDENTIAL


ABSTRACT

The results of subsonic wind tunnel flutter tests on a dynamic model of an unswept all-movable horizontal tail are presented. The test data show the variation of flutter speed with stabilizer rotational restraint for three positions of the rotational axis. In addition, the effect of free-play in the stabilizer actuating mechanism on the flutter speed is determined for one rotational frequency at one rotational axis position. Complete model data, including the measured zero airspeed coupled vibration frequencies and node lines, are included.

PUBLICATION REVIEW

This report has been reviewed and is approved.

FOR THE COMMANDER:

for 
DANIEL D. MCKEE
Colonel, USAF
Chief, Aircraft Laboratory
Directorate of Laboratories

WADC TR 54-53

iii

CONFIDENTIAL

CONFIDENTIAL

TABLE OF CONTENTS

Introduction		Page
I	Model Design and Construction	1
II	Tail Rotation Mechanism	3
III	Mass and Elastic Data	6
IV	Vibration and Flutter Test Data	10
V	Discussion of Results	13
VI	Concluding Remarks	21

CONFIDENTIAL

CONFIDENTIAL

LIST OF TABLES

	Page
I Mass and Inertia Data	7
II Structural Influence Coefficients	8
III . Vibration and Flutter Test Data	11

CONFIDENTIAL

CONFIDENTIAL

LIST OF ILLUSTRATIONS

Figure	Page
1. Planform of Unswept All-Movable Tail	2
2. Model Mounted in Wind Tunnel	4
3. Top View of Tail Rotation Mechanism	5
4. Spar Support Block	5
5. Operating Parts of Tail Rotation Mechanism	5
6. Test Set-Up for Measuring Bending Influence	
Coefficients	9
7. Reduced Flutter Speed as a Function of Frequency	
Ratio, $\frac{V}{b_0 \omega_\alpha}$ vs. $\frac{\omega_\delta}{\omega_\alpha}$	14
8. Reduced Flutter Speed as a Function of Frequency	
Ratio, $\frac{V}{b_0 \omega_r}$ vs. $\frac{\omega_\delta}{\omega_\alpha}$	15
9. Reduced Flutter Speed as a Function of Frequency	
Ratio, $\frac{V}{b_0 \omega_r}$ vs. $\frac{\omega_r}{\omega_\alpha}$	16
10. Flutter Speed Ratio as a Function of Frequency	
Ratio, $\frac{V}{V_L}$ vs. $\frac{\omega_\delta}{\omega_\alpha}$	18
11. Flutter Speed Ratio as a Function of Frequency	
Ratio, $\frac{V}{V_L}$ vs. $\frac{\omega_r}{\omega_\alpha}$	19
12. Flutter Speed Ratio $\frac{V}{V_0}$ as a Function of	
Angular Free Play	20
13 to 34. Zero Airspeed Vibration Node Lines and Frequencies	22 to 27

CONFIDENTIAL

INTRODUCTION

The current use of all-movable horizontal tails in place of the more conventional stabilizer-elevator combination has introduced some new flutter problems to the aircraft designer. In particular he needs to know how stiff the actuating mechanism of an all-movable tail must be in order to insure freedom from flutter, and what amount of stabilizer rotational free play can be tolerated before a normally safe configuration becomes dangerous from the flutter standpoint. In order to provide answers to questions such as these, the Aircraft Laboratory of the Wright Air Development Center initiated a project to investigate the flutter characteristics of all-movable tails. The first phase of this project, subsonic wind tunnel tests of an unswept stabilizer flutter model, is reported here. Subsequent phases will include subsonic tests of a swept back model and transonic tests.

The present investigation consisted of two parts. First, a series of tests were conducted to determine the effect of varying the rotational restraint of an all-movable stabilizer on the flutter speed. These tests were performed for three locations of the axis of rotation. A second series of tests were then run to determine the influence of stabilizer rotational free play on the flutter characteristics of a particular case. This report presents a description of the model including its mass and elastic properties, the zero airspeed vibration modes and frequencies for all configurations tested in the wind tunnel, and finally the wind tunnel flutter data.

The vertical bending of a fuselage was not simulated in the model used for this investigation. This mode of vibration is expected to influence the flutter test data appreciably for low rotational frequencies of the all-movable tail. The Wright Air Development Center plans to investigate this effect by further wind tunnel tests in a future phase of the all-movable stabilizer flutter research program.

CONFIDENTIAL

CONFIDENTIAL

I. MODEL DESIGN AND CONSTRUCTION

A single spar flutter model was designed to simulate a conventional unswept horizontal stabilizer. The planform of the model is shown in Figure 1 and various geometric data are listed on this Figure. The model was set in the wind tunnel so that the spar, located at 33 percent of the wing chord, was normal to the airstream direction. The spar was machined out of dural and had a rectangular cross section which tapered uniformly from root to tip. Eight four-inch wide sections were attached to the spar, each section consisting of a pair of ribs, a balsa sheet which formed the leading edge, a solid balsa trailing edge piece, and a doped silk covering. The ribs were constructed of a balsa framework into which was pressed and glued a plywood core. The spar fitted tightly through a slot in the core. Every section was anchored to the spar at each of its ribs so that it was structurally independent of adjacent sections. The space between sections was covered with a very thin sheet of rubber glued to the two adjacent sections. By this type of construction the elastic properties of the model were concentrated primarily in the spar. The elastic axis was found to coincide with the spar during structural stiffness tests of the model.

The model was designed to have a mass ratio of 20 and a center of gravity location of 45 percent of the chord aft of the leading edge. To achieve these mass properties lead weights were fastened to the ribs of each section, forward and aft of the spar. The resulting radius of gyration of each section about the elastic axis varied from 33 to 40 percent of the local chord. Three locations for the axis of rotation of the tail were available: 24.34%, 33.00%, and 41.66% of the mean aerodynamic chord. Details about the mechanism which provided rotational freedom for the model are presented in the next section.

The model incorporated the following instrumentation: two sets of strain gages were located on the spar at the stabilizer root, arranged to pick up bending and torsion strains separately.

CONFIDENTIAL

CONFIDENTIAL

Model Data:
 Area: 532 in²
 Geometric A/R: 1.92
 Taper Ratio: 0.541
 Airfoil: NACA 0010
 Spar located at 33%
 of wing-chord (constant
 along span).

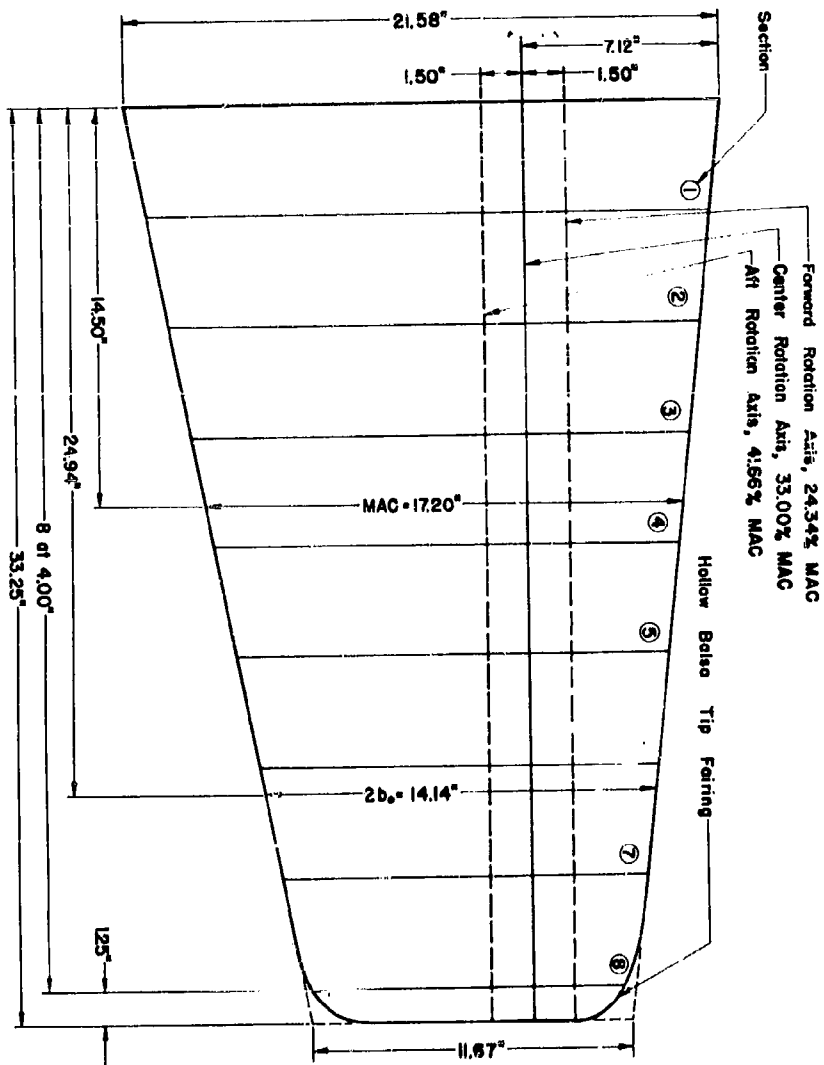


Figure 1
Planform of Unswept All-Movable Tail

CONFIDENTIAL

CONFIDENTIAL

A Statham accelerometer was mounted on the inboard rib of the second section of the model, about four inches aft of the spar. The outputs of these instruments were fed thru a 3 KC Consolidated Amplifier into a Brush Recorder. During actual testing only two of the three pickups were recorded simultaneously. The completed model mounted in the WADC Five Foot Wind Tunnel is shown in Figure 2.

II. TAIL ROTATION MECHANISM

Figures 3 and 4 are photographs of the top of the rotation mechanism and the spar support block respectively, and Figure 5 is a sketch showing the assembly of the mechanism. Corresponding numbers on the three Figures cross reference the various parts. The mechanism operates in the following manner. A leaf spring (2) is fastened in clamps (1) and (3). The upper clamp (1) is rigidly attached to the framework, while the lower clamp (3) is fastened to a shaft (5) which is supported by two sets of bearings (7) (only the bottom set is shown in Figures 4 and 5). The bearing housing (6) is bolted to the framework. The lower end of the shaft is rigidly connected to the spar support block (8), and the model is then attached by clamping the spar (9) in one of the slots in the lower surface of the spar support block. This arrangement allows the lower spring clamp, the shaft, the spar support block, and the model to rotate against the spring about the axis of the shaft. The axis of rotation of the movable tail can be changed by clamping the spar in any one of the three slots in the spar support block. The rotation frequency of the tail can be varied by changing springs. The large bolts (4) limit the rotation amplitude and also can be used to lock the mechanism at the lower spring clamp.

To obtain a given amount of free play in the rotation mechanism, shims a little thicker than the spring are placed on each side of the spring at the upper clamp, and the clamp is drawn up tight on the shims. This arrangement allows the mechanism to rotate freely a specified amount before the spring contacts the upper clamp and becomes effective in restraining the motion. The amount of free-play in the system is thus governed by the difference in thickness between the spring and the shims.

CONFIDENTIAL

CONFIDENTIAL

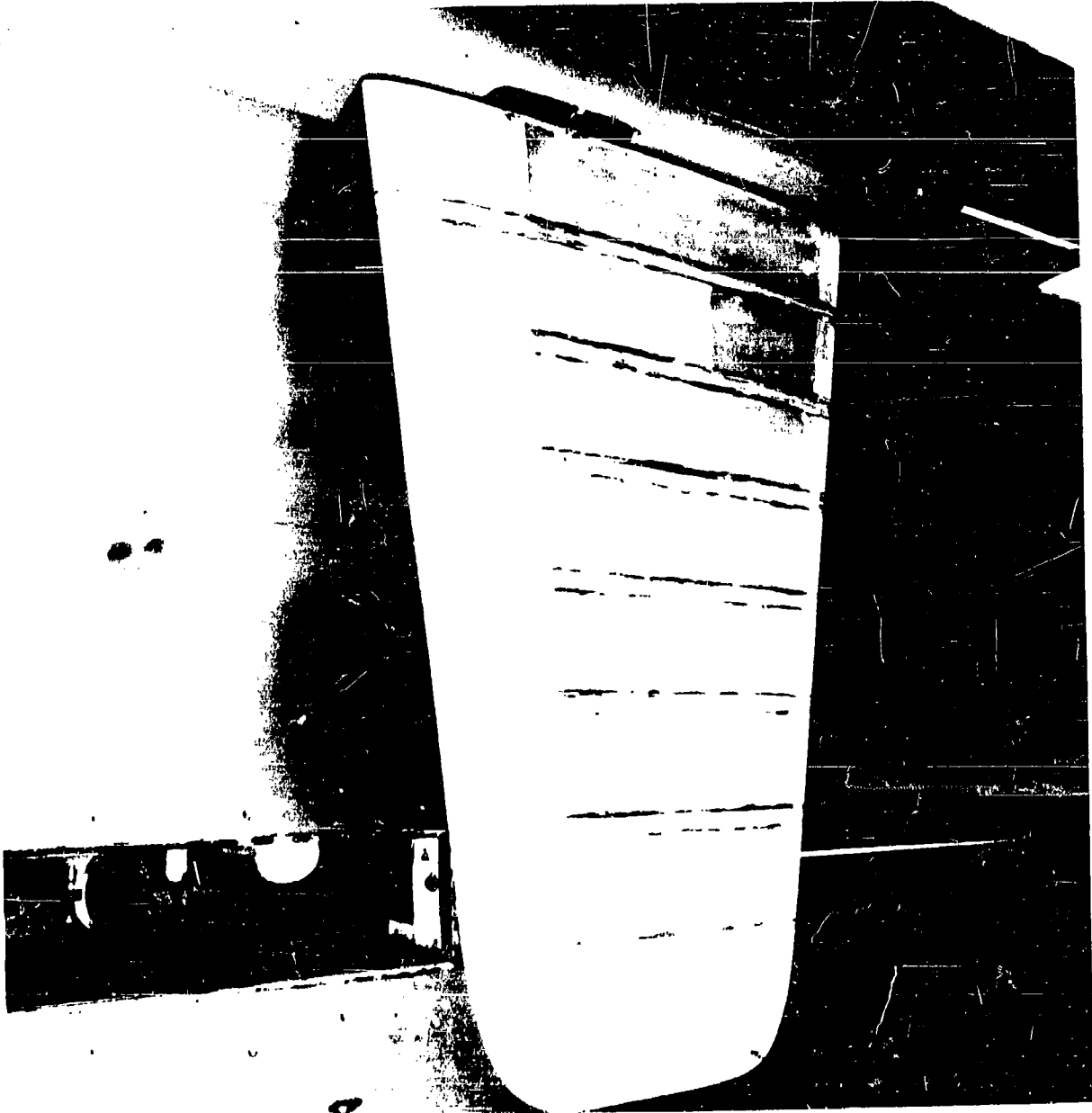


Figure 2
Model Mounted in the Wind Tunnel

CONFIDENTIAL

CONFIDENTIAL

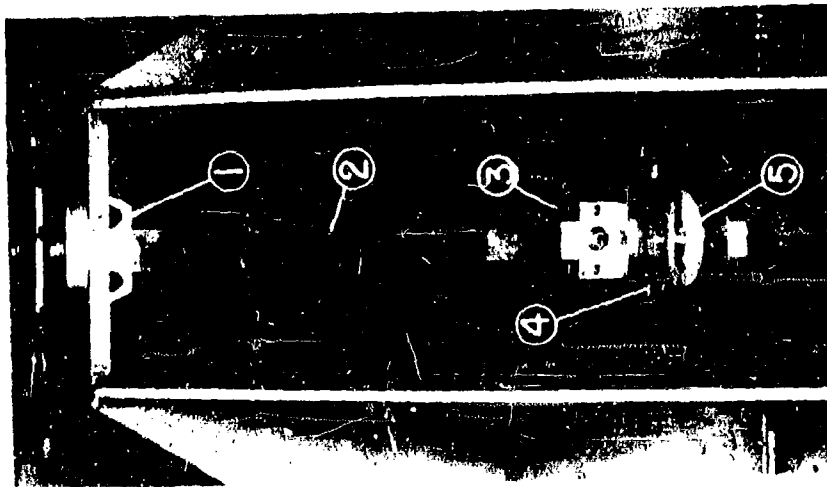


Figure 3
Top View of Tail Rotation Mechanism

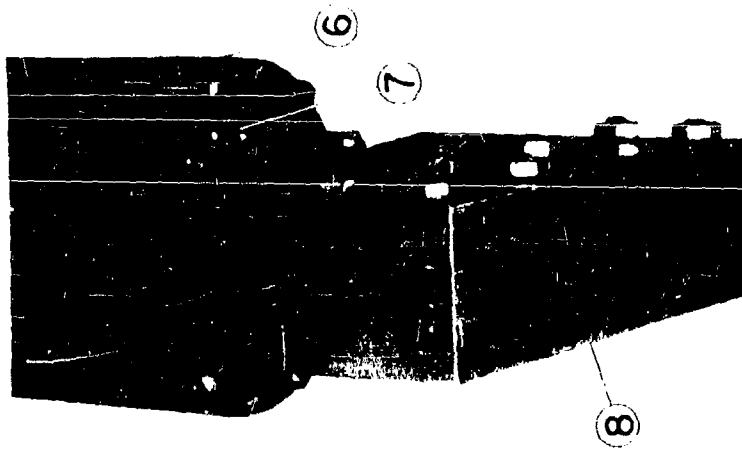


Figure 4
Spar Support Block

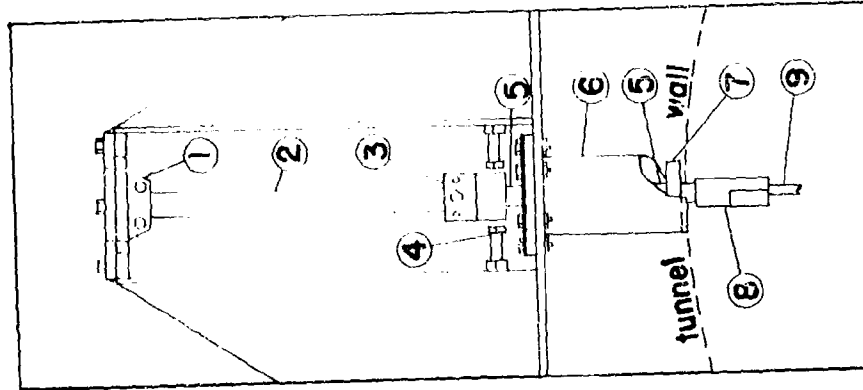


Figure 5
Operating Parts
of
Tail Rotation Mechanism

CONFIDENTIAL

CONFIDENTIAL

III. MASS AND ELASTIC DATA

Table 1 summarizes the mass and inertia data for each section of the model. Before the model was assembled each section was weighed and then swung to measure its static unbalance ($S_x \Delta y$) and moment of inertia ($I_x \Delta y$) about the spar center-line (wing elastic axis). With these parameters known, the mass unbalance about each rotation axis ($S_y \Delta y$), the product of inertia about the rotation axis and the elastic axis ($P_{xy} \Delta y$), and the moment of inertia about the rotation axis ($I_y \Delta y$) were calculated. The c.g. location and mass ratio are tabulated to indicate how nearly the model met its design requirements. A separate measurement was made of the moment of inertia of the spar block, shaft, and lower spring clamp of the rotation mechanism about the axis of the shaft. This measured value was 0.04303 pound-feet². Comparing this with the moment of inertia of the complete wing about each of the rotation axes (obtained as the sums of the sectional inertias), it is seen that the rotation mechanism constituted at most 2.7% of the total inertia.

The elastic characteristics of the stabilizer model itself were determined by measuring the bending and torsion influence coefficients. The data are presented in Table II, and Figure 6 is a photograph of the set-up for the bending influence coefficient measurements. For both tests the spar was clamped at the root of the stabilizer so that the model was effectively cantilevered. From the data of the torsion test it was noted that the axis about which the stabilizer twisted very nearly coincided with the center line of the spar. Also, from the bending test, when loads were applied along the spar a pair of scales forward and aft of the spar at the tip showed equal deflections. From these results it was decided that for all practical purposes the elastic axis coincided with the spar center-line (33% wing chord).

Using the influence coefficients and the mass data, the cantilever uncoupled bending and torsion modes of the stabilizer were computed. The amplitude distributions and frequencies are presented in Table I.

CONFIDENTIAL

CONFIDENTIAL

TABLE I
Mass and Inertia Data

Sec- tion	Wing Sta- tion, Y, (inches)	b(Y) (feet)	h ₁ (Y) (Pounds)	S ₁ AY (lb-ft)	I ₁ AY (lb-ft ²)	C.G. (% Chord)	Mass Ratio μ	Rad. of Gyr. About E.A. (% Chord)	h ₁ (Y) (218 GPM)
1	2	.871	1.24	.268	.412	45.4	20.4	33.1	.00673
2	6	.818	1.05	.291	.437	50.0	19.6	39.5	.0515
3	10	.767	.964	.181	.272	45.3	20.4	34.7	.127
4	14	.717	.862	.161	.230	46.0	20.9	36.1	.242
5	18	.664	.733	.122	.157	45.5	20.7	34.8	.397
6	22	.614	.628	.0884	.143	44.5	20.8	38.9	.578
7	26	.566	.634	.0854	.115	44.9	24.7	37.6	.788
8	30	.513	.457	.0598	.0555	47.0	21.6	33.9	1.00
$\Sigma = 6.57$					$\Sigma = 1.82$				

Sec- tion	h ₂ (Y) (997 GPM)	α_1 (Y) (706 GPM)	α_2 (Y) (1520 GPM)	Rotation axis at 24.3% MAC			Rotation axis at 41.7% MAC		
				S ₁ AY (lb-ft)	P ₁ AY (lb-ft ²)	I ₁ AY (lb-ft ²)	S ₂ AY (lb-ft)	P ₂ AY (lb-ft ²)	I ₂ AY (lb-ft ²)
1	-.0438	.0548	-.124	.423	.445	.498	.112	.378	.364
2	-.230	.182	-.378	.422	.473	.526	.160	.400	.380
3	-.563	.329	-.519	.302	.295	.333	.0606	.250	.242
4	-.615	.489	-.490	.269	.250	.284	.0531	.210	.204
5	-.719	.649	-.234	.214	.172	.199	.0305	.142	.138
6	-.667	.810	.217	.167	.154	.175	.00988	.132	.131
7	.265	.939	.720	.165	.126	.146	.00620	.104	.104
8	1.00	1.00	1.00	.117	.0629	.0775	.00274	.0480	.0476
$\Sigma = 2.24$					$\Sigma = 1.61$				

CONFIDENTIAL

CONFIDENTIAL

TABLE II
STRUCTURAL INFLUENCE COEFFICIENTS

Torsion (Radians/Foot-Pound)

	Wing-Section							
	1	2	3	4	5	6	7	8
	Station Distance from Root (in.)							
	2	6	10	14	18	22	26	30
Wing Section 1	.00047	.00047	.00047	.00047	.00047	.00047	.00047	.00047
2	.00047	.00160	.00160	.00160	.00160	.00160	.00160	.00160
3	.00047	.00160	.00308	.00308	.00308	.00308	.00308	.00308
4	.00047	.00160	.00308	.00499	.00499	.00499	.00499	.00499
5	.00047	.00160	.00308	.00499	.00745	.00745	.00745	.00745
6	.00047	.00160	.00308	.00499	.00745	.0109	.0109	.0109
7	.00047	.00160	.00308	.00499	.00745	.0109	.0155	.0155
8	.00047	.00160	.00308	.00499	.00745	.0109	.0155	.0220

Bending (Feet/Pound x 10⁻³)

	Wing-Section							
	1	2	3	4	5	6	7	8
	Station Distance from Root (in)							
	2	6	10	14	18	22	26	30
Wing Section 1	.00833	.0533	.108	.125	.175	.217	.233	.275
2	.0533	.333	.592	.950	1.29	1.48	1.96	2.22
3	.108	.592	1.38	2.33	3.10	3.94	4.63	5.44
4	.125	.950	2.33	3.25	5.58	7.42	9.17	10.9
5	.175	1.29	3.10	5.58	8.75	12.0	14.9	18.6
6	.217	1.48	3.94	7.42	12.0	17.0	22.4	27.6
7	.233	1.96	4.63	9.17	14.9	22.4	31.3	38.9
8	.275	2.22	5.44	10.9	18.6	27.6	38.9	51.7

CONFIDENTIAL



Figure 6
Test Set-Up for Measuring Bending Influence Coefficients

WADC TR 54-53

9

CONFIDENTIAL

CONFIDENTIAL

The springs used in the rotation mechanism to vary the rotation frequency of the tail were uniform steel bars, 12 inches in length between clamps, 1 inch wide, and of varying thickness. The torsional stiffness of each spring was measured while it was mounted in the rotation mechanism. On comparing the measured values with the calculated torsional stiffnesses of the leaf springs alone, it was found that the rotation mechanism introduced appreciable flexibility. Using the measured rotational stiffnesses and the calculated moments of inertia of the complete movable tail, the uncoupled tail rotational frequencies (ω_p) were calculated and are listed in Table III.

IV. VIBRATION AND FLUTTER TEST DATA

The test results of the unswept all-movable tail flutter model are presented in Table III. Preceding each wind tunnel run a vibration test was conducted to measure the zero airspeed normal modes of vibration. The mode lines and frequencies are shown in Figures 14 to 34, and the frequencies are also tabulated in Table III. Figure 13 shows the cantilever modes of the model, which were measured prior to installing the model in the rotation mechanism. In every case tested, the model exhibited a vibration mode which was primarily fore and aft bending, occurring at a frequency slightly below that of the second bending mode. Although at zero airspeed the fore and aft bending mode seemed to involve a slight coupling with torsion, during the flutter tests no fore and aft motion could be detected by eye.

The flutter data were obtained in two series of tests: first, for each rotation axis location, the model was fluttered with different springs in the rotation mechanism; then, for the 33% MAC rotation axis and with only one of the moderately stiff springs (0.24 inches thick), various amounts of free play were introduced in the rotation mechanism and flutter tests were repeated. Manual excitation by means of cords attached to the stabilizer tip at leading and trailing edges was used to initiate flutter. The critical flutter speed was determined as the lowest speed at which constant amplitude oscillations sustained themselves. In a number of cases it was found that flutter could be induced at

CONFIDENTIAL

CONFIDENTIAL

CONFIDENTIAL

TABLE III
VIBRATION AND FLUTTER TEST DATA

Run No.	Rotation Axis Location (% MAC)	Spring Thickness (Inches)	Uncoupled Rotation Frequency (ω_u , CPM)	Free Play (Degrees)	Zero Airspeed Frequencies, CPM				Flutter Speed, V (KAS, MPH)	Flutter Frequency ω_f (CPM)	$\left(\frac{V}{b \omega_f}\right)^*$	$\left(\frac{V}{b \omega_f}\right)^{**}$	$\left(\frac{\omega_f}{\omega_u}\right)$	$\left(\frac{\omega_f}{\omega_u}\right)$
					1st Mode	2nd Mode	3rd Mode	4th Mode						
0	—	C	∞	0	242	796 T	968	991	—	—	—	—	—	—
1	24.34	L	2489	0	242	745 T	817	1007	131.2	475	6.53	4.42	3.54	1.06
2	24.34	0.36	1115	0	262	662 T	818	994	119.8	441	6.48	4.38	1.58	0.928
3	24.34	0.24	610	0	259	536 T	816	1000	97.2	378	6.11	3.27	0.384	0.753
4	24.34	0.18	438	0	250	420 T	808	987	69.4	319	5.17	2.33	0.320	0.585
5	24.34	0.12	244	0	208	295 T	832	984	32.8	254	3.07	1.10	0.342	0.418
6	24.34	0.10	187	0	170 T	279	828	993	34.0	237	3.41	1.14	0.365	0.241
7	33.00	L	2766	0	280	768 T	840	1008	140.2	486	7.15	4.71	3.52	1.11
8	33.00	0.36	1128	0	263	690 T	840	1028	126.9	434	6.82	4.27	1.50	0.977
9	33.00	0.30	824	0	268	635 T	857	1000	115.1	413	6.63	3.88	1.31	0.885
10	33.00	0.24	674	0	265	558 T	842	988	99.2	375	6.29	3.34	0.965	0.793
11	33.00	0.18	484	0	256	433 T	833	994	72.2	324	5.31	2.43	0.930	0.613
12	33.00	0.12	270	0	229	305 T	833	1000	28.6	255	2.87	0.96	0.382	0.432
13	33.00	0.10	207	0	193 T	285	833	1000	32.9	231	3.39	1.11	0.282	0.273
14	33.00	0.08	147	0	147 T	238	850	1012	50 D	—	—	—	—	—
15	33.00	0.06	103	0	128 T	255	841	1000	35 D	—	—	—	—	—
16	41.66	L	2939	0	250	741 T	788	931	130.2	478	6.48	4.39	4.18	1.06
17	41.66	0.36	1198	0	254	672 T	791	978	117.8	435	6.44	3.87	1.70	0.962
18	41.66	0.24	716	0	240	553 T	818	987	95.7	375	6.07	3.23	1.01	0.783
19	41.66	0.18	514	0	256	441 T	812	971	74.0	317	5.55	2.49	0.723	0.625
20	41.66	0.12	287	0	241	281 T	812	981	34.7	246	3.35	1.17	0.407	0.398
21	41.66	0.10	219	0	211 T	262	812	988	51 D	—	—	—	—	—
22	33.00	0.24	874	0	—	—	—	—	87.1	375	6.18	3.28	0.955	—
23	33.00	0.24	874	1.52	—	—	—	—	35.4	262	3.22	1.20	0.955	—
24	33.00	0.24	874	0.62	—	—	—	—	38.5	297	3.44	1.30	0.955	—
25	33.00	0.24	874	0.29	—	—	—	—	49.9	289	4.11	1.88	0.955	—
26	33.00	0.24	874	0.08	—	—	—	—	77.8	321	5.78	2.62	0.955	—
27	33.00	0.24	874	0.04	—	—	—	—	82.5	346	6.01	3.12	0.955	—
28	33.00	0.24	874	0	—	—	—	—	93.1	379	6.15	3.31	0.955	—

NOTES: C - Model cantilevered by clamping spar at stabilizer root.
L - Rotation mechanism locked by locking bolts at lower spring clamp.
D - Model diverged before flutter occurred.
P - Fore and aft bending mode of model.
T - Vibration mode with node line most nearly resembling a conventional torsion mode.
* - $b_0 = \text{ref.} = 0.588 \text{ feet}$ reference station at 75% of the span from the root.
** - ω_u = calculated uncoupled cantilever torsion frequency = 700 cpm.
 ω_f - Frequency of mode corresponding to note "T" above.

CONFIDENTIAL

CONFIDENTIAL

CONFIDENTIAL

lower speeds than those reported in Table III by exciting the model and then holding one of the cords taut. The frequency and mode of flutter under such circumstances were different than under normal conditions. Care was taken to insure that the cord was always set free following an excitation, in approaching the true flutter speed.

For the free play tests, the problem of determining the critical flutter speed was more difficult. For example: with the largest amount of free play (Run No. 23, Table III), constant amplitude flutter occurred at 31.2 mph in which the model pitching amplitude was slightly less than the amplitude of the free play. However, if the model was excited thru a large enough amplitude to rotate it through the free play and deflect the spring, then the ensuing oscillations would damp down until they were again within the free play range and persist at that amplitude. The frequency of the "free play flutter" was 234 cpm. At a slightly higher speed of 35.4 mph, constant amplitude flutter was obtained in which the model rotated through the total travel allowed by the free play and banged the spring against the stops in the upper clamp. The frequency of this flutter was 262 cpm.

With the next smaller amount of free play (Run No. 24), constant amplitude flutter was obtained at 38.5 mph at a frequency of 267 cpm in which the spring was just contacting the stops in the upper clamp during its rotational motion. It was possible to raise the wind tunnel speed to over 50 mph and the flutter oscillations were still non-divergent although the amplitude tended to increase with airspeed. The flutter frequency had increased to 288 cpm at this higher speed. The test was stopped at this point to avoid possible damage to the model.

As the amount of free play was successively decreased, the flutter characteristics of the model tended to become more nearly like those of the no-free-play case. The flutter was more violent than with larger amounts of free play and the flutter speed was higher although it was still below the critical speed without free play. The only unusual behavior noted was that at speeds below the critical flutter speed the damping envelope of the decaying oscillations would change character depending on the strength of the initial excitation; also the rate of decay was lower for stronger excitation. However, the actual critical flutter speed appeared to be independent of the applied impulse. In all free-play cases, the flutter mode appeared to be stabilizer rotation vs. stabilizer bending.

CONFIDENTIAL

CONFIDENTIAL

During Runs 14, 15, and 21, when very weak springs were used in the rotation mechanism, the model diverged before flutter occurred. The amplitude was limited by the locking bolts of the rotation mechanism (see Figure 3) so that no damage occurred. It may be remarked that during the design of the model, the divergence speed of the cantilevered stabilizer was calculated to be 246 mph.

V. DISCUSSION OF RESULTS

In order to facilitate interpretation of the results, the test data have been plotted in several forms in Figures 7 thru 12. Figure 7 shows the reduced flutter speed, $V/b_0\omega_\alpha$, plotted against the ratio of computed uncoupled rotation frequency, ω_β , to computed uncoupled cantilever torsion frequency, ω_α ($= 706$ cpm). The abscissa, therefore, represents a parameter which presumably would be computed or estimated during the design of an all-movable horizontal tail. Aside from the expected lowering of the flutter speed as the rotation frequency is reduced, it may be seen that, for any given value of the frequency ratio $\omega_\beta/\omega_\alpha$, the location of the rotation axis does not significantly influence the flutter speed. It is interesting to note that as the rotation frequency is further reduced, the flutter speed tends to rise again. This trend appears to continue, as the data of Table III indicate, until divergence rather than flutter becomes the critical phenomenon.

An alternative way of presenting the same data is shown in Figure 8. Here the flutter speed is non-dimensionalized by the product of the reference semichord and the frequency of the measured coupled vibration mode which has a node line most nearly resembling a torsion mode, ω_T . The abscissa is again the computed uncoupled frequency ratio $\omega_\beta/\omega_\alpha$. This curve shows that for values of $\omega_\beta/\omega_\alpha$ greater than about 0.8, the flutter speed is essentially proportional to ω_T .

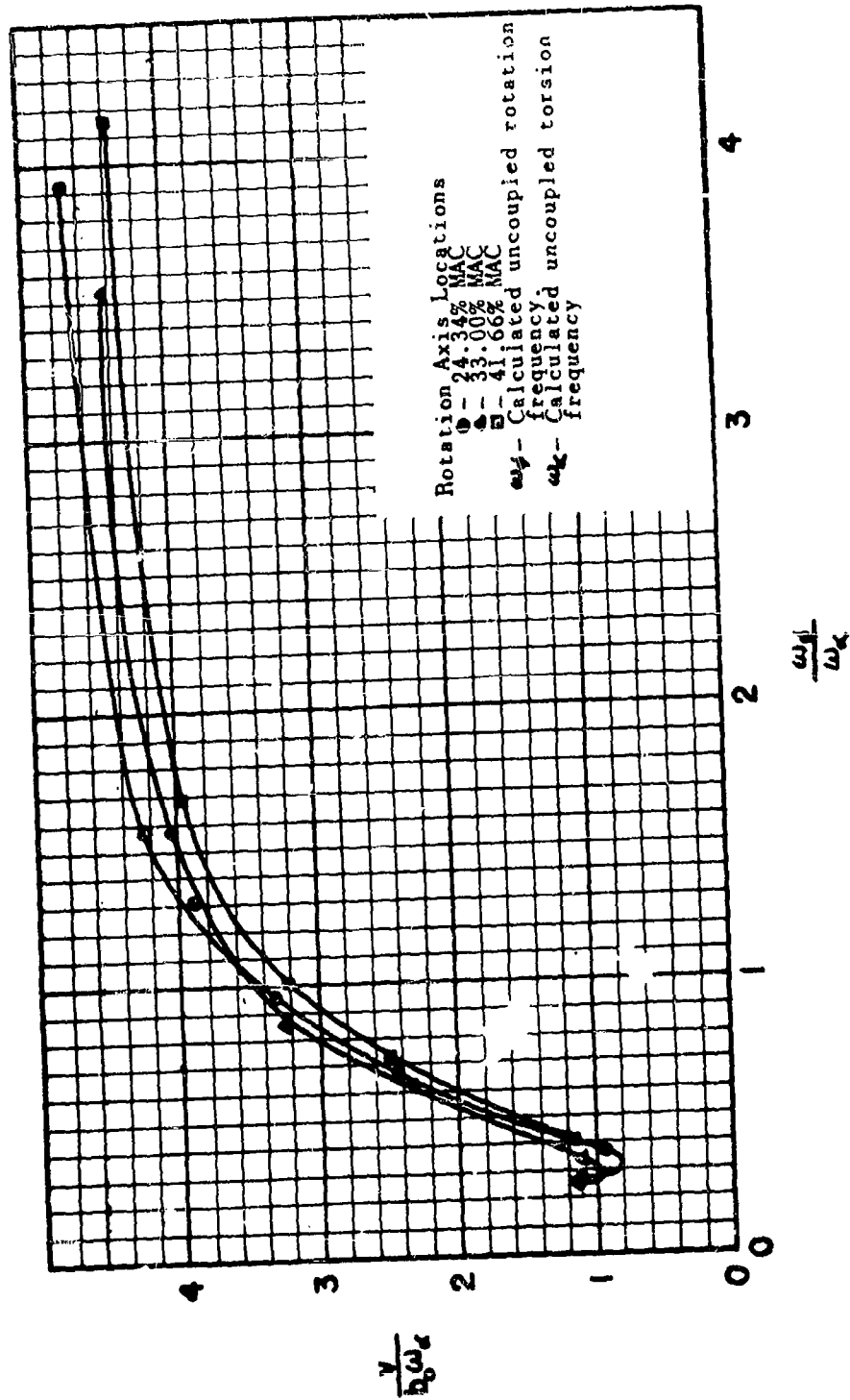
Figure 9 presents the experimental data in a form which may be useful after an all-movable tail has been built and a vibration test conducted. In such a case the measured frequency of the torsion-rotation mode, ω_T , would be known. The curves then give an estimate of the flutter speed to be expected for configurations similar to the present one for subsonic flight conditions. In general no difficulty was encountered in identifying the mode to

CONFIDENTIAL

CONFIDENTIAL

Figure 7

Reduced Flutter Speed $\frac{V}{b_0 \omega_c}$ as a Function
of Frequency Ratio $\frac{\omega_f}{\omega_c}$



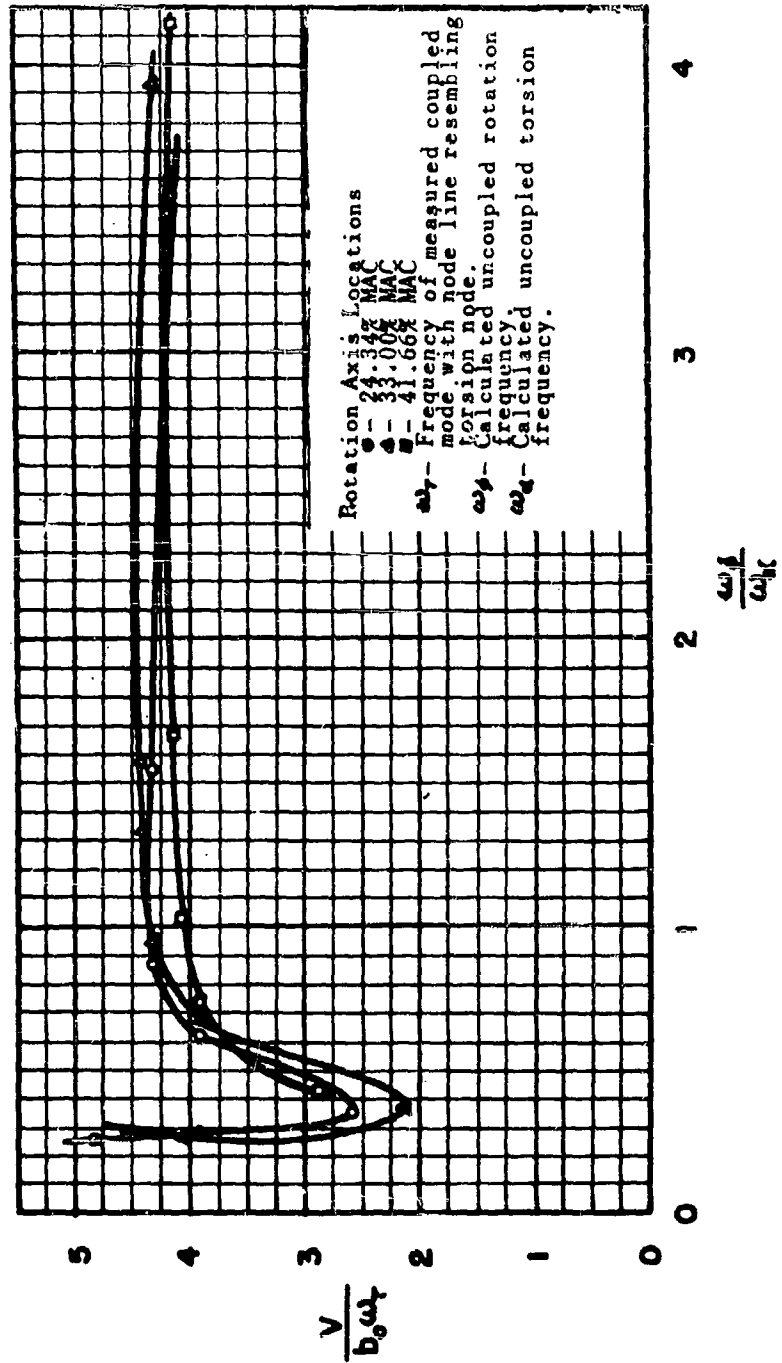
WADC TR 54-53

11

CONFIDENTIAL

CONFIDENTIAL

Figure 8
Reduced Flutter Speed $\frac{V}{b_0 \omega_f}$ as a Function
of Frequency Ratio $\frac{\omega_f}{\omega_k}$



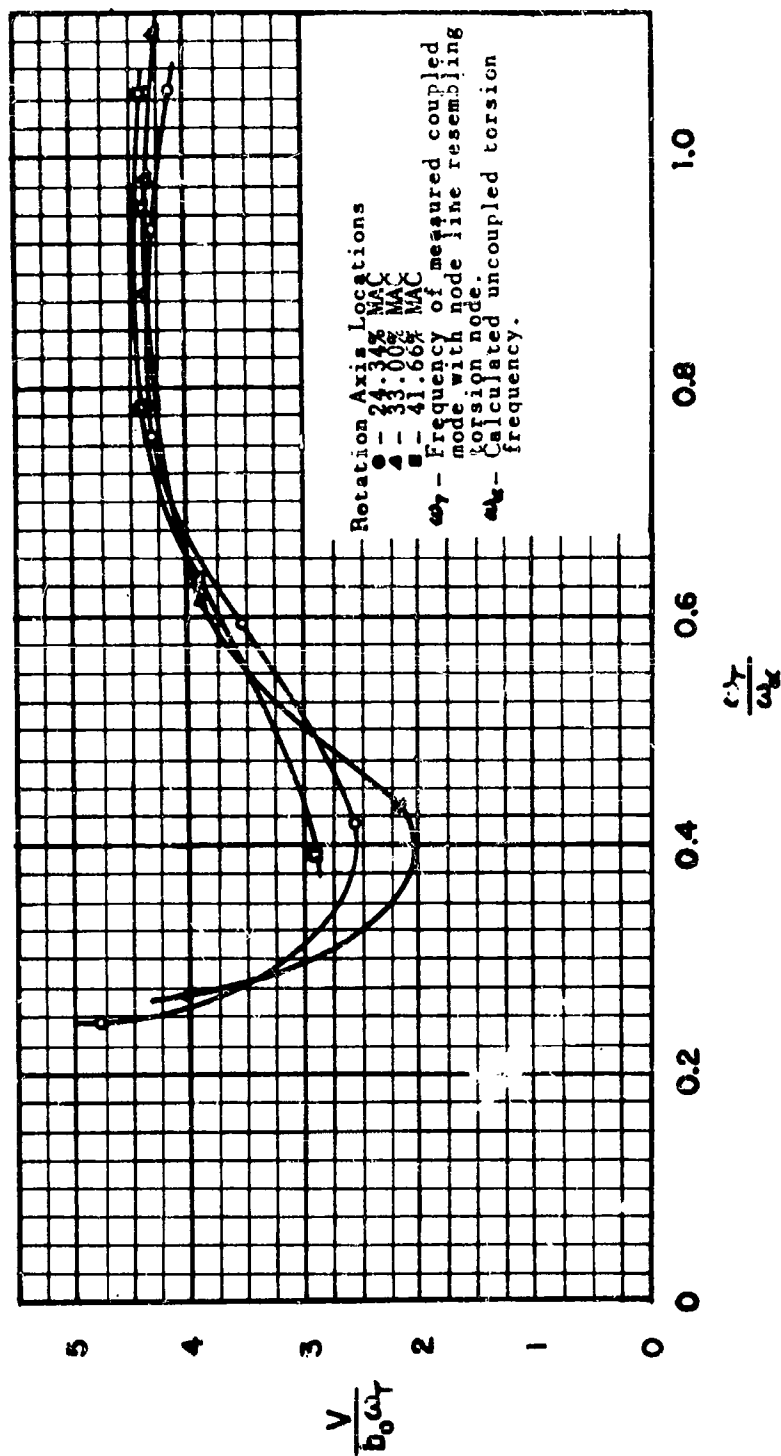
WADC TR 54-53

15

CONFIDENTIAL

CONFIDENTIAL

Figure 9
Reduced Flutter Speed $\frac{V}{b_0 \omega_T}$ as a Function
of Frequency Ratio $\frac{\omega_T}{\omega_k}$



CONFIDENTIAL

CONFIDENTIAL

be defined as the torsion-rotation mode since there normally was only one mode whose node line ran essentially in the spanwise direction. However, as the uncoupled rotation frequency approaches the cantilever first bending frequency, a pair of coupled vibration modes are obtained both of whose node lines can be considered as nearly spanwise. This can be seen in Figures 18, 19, and 25, corresponding to Runs 5, 6, and 12 respectively. In these cases, the torsion-rotation mode was arbitrarily selected as that one whose node line crossed the edge of the wing at the furthest outboard station.

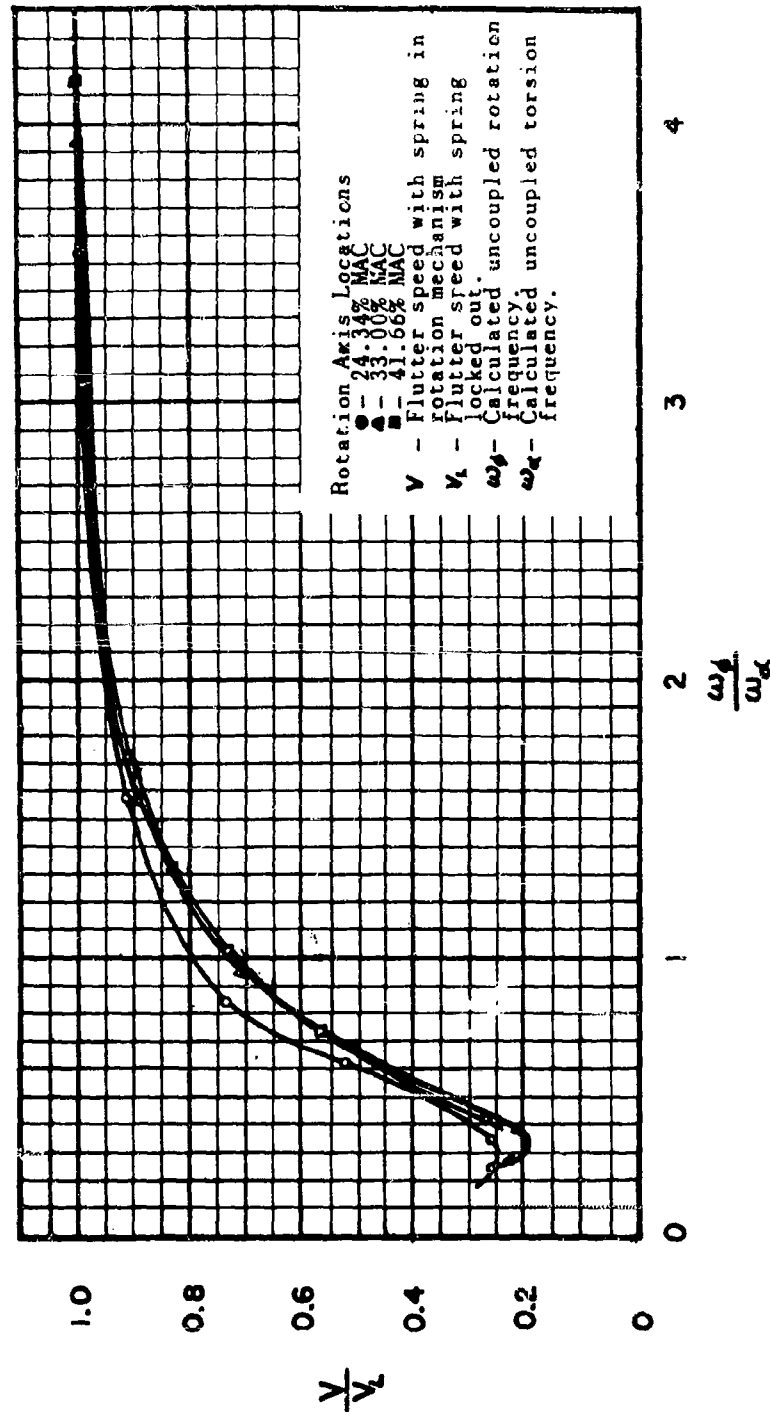
Figures 10 and 11 plot the ratio of the flutter speed with flexibility in the rotation mechanism (V) to the flutter speed with the rotation mechanism locked at the lower spring clamp (V_L), against the ratios $\omega_\phi/\omega_\alpha$ and ω_r/ω_α respectively. These curves indicate to what extent the flutter speed of an all-movable tail will be lowered if the actuating mechanism is not sufficiently stiff. Even when the computed frequency of the (rigid) tail rotating against the actuator spring is 1-1/2 times the uncoupled torsion frequency of the tail, the flutter speed is of the order of 10 per cent less than its potential maximum value with no flexibility in the rotation mechanism. Here again it can be seen that the results are slightly affected by the location of the rotation axis.

The effect of free-play in the actuating system of an all-movable tail is shown in Figure 12. This curve pertains to the case where the rotation axis is at 33% MAC and the frequency ratio $\omega_\phi/\omega_\alpha = 0.955$. For this case the first 1/20 of a degree of free-play introduced into the system results in a reduction in flutter speed of approximately 10 percent. The decrease in flutter speed continues until about 0.6 degrees of free play, after which there appears to be little further change. However, at this point the flutter speed is only about 40% of the value with no play.

CONFIDENTIAL

CONFIDENTIAL

Figure 10
Flutter Speed Ratio $\frac{V}{V_L}$ as a Function of
Frequency Ratio $\frac{\omega_1}{\omega_2}$



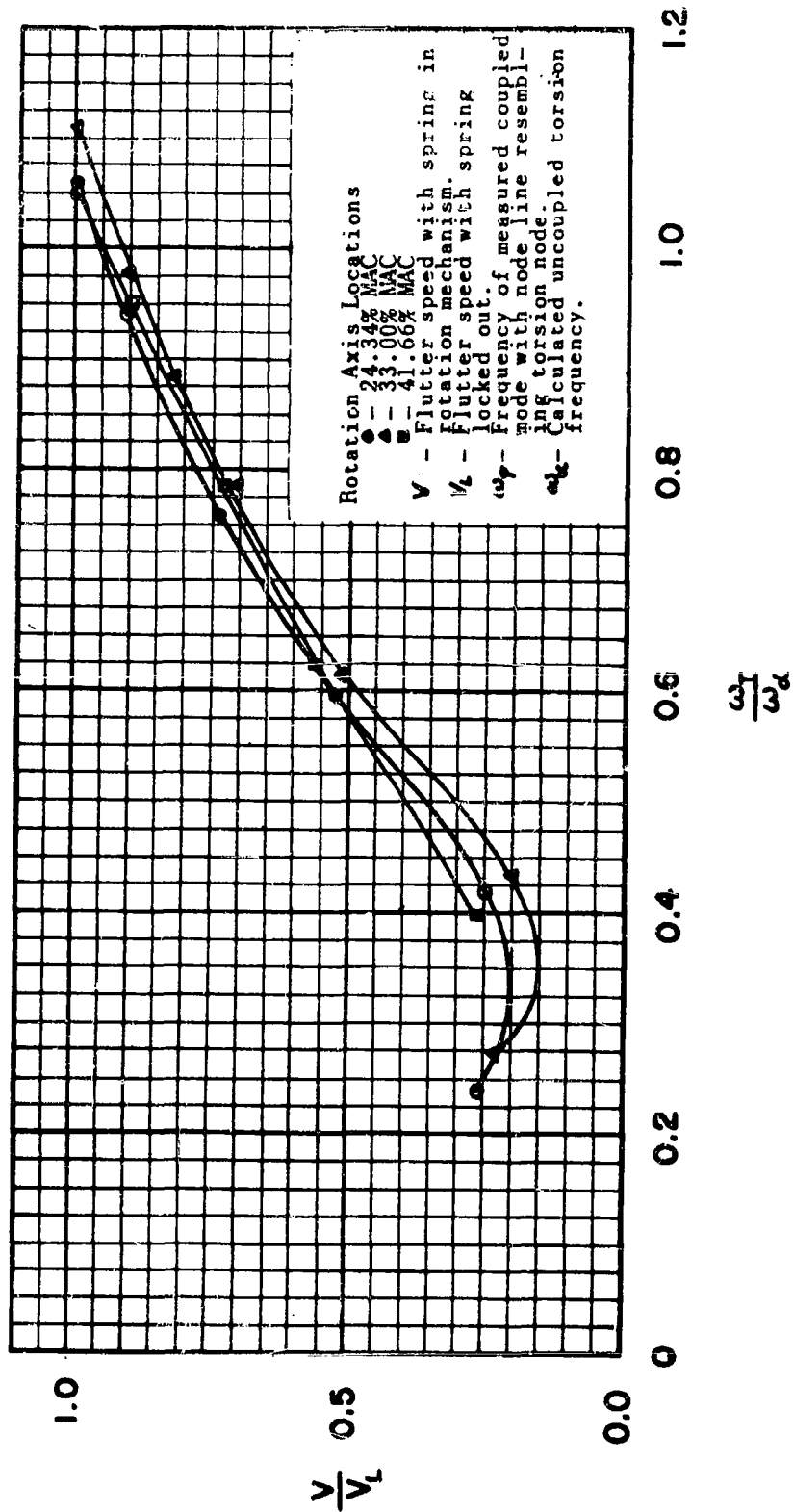
WADC TR 54-53

18

CONFIDENTIAL

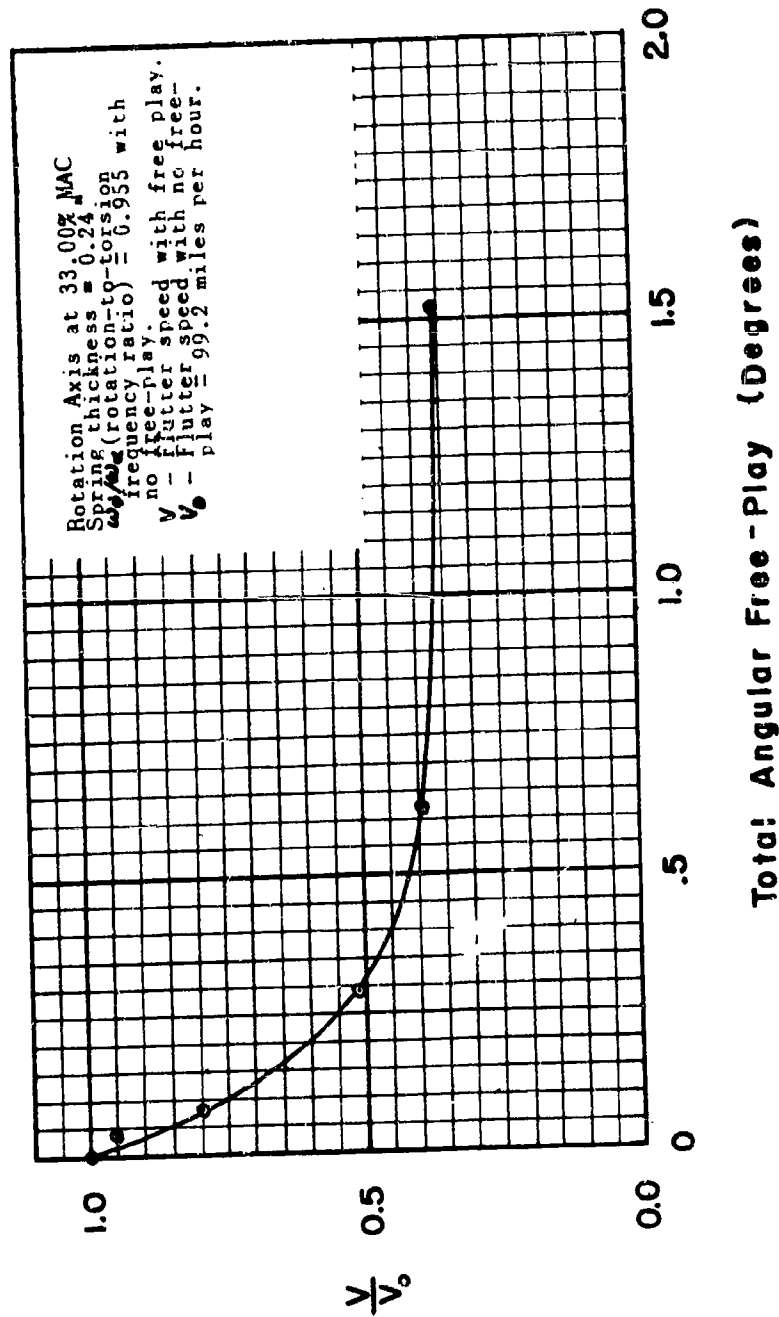
CONFIDENTIAL

Figure II
Flutter Speed Ratio $\frac{V}{V_L}$ as a Function
of Frequency Ratio $\frac{\omega_T}{\omega_A}$



CONFIDENTIAL

Figure 12
Flutter Speed Ratio $\frac{V}{V_0}$ as a Function
of Angular Free-Play



WADC TR 54-53

CONFIDENTIAL

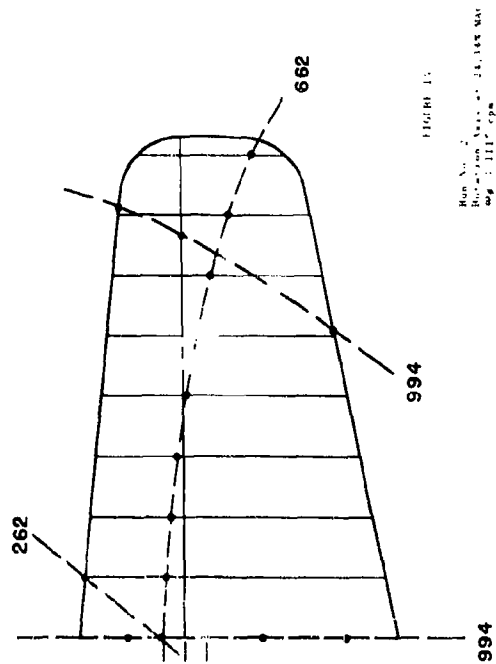
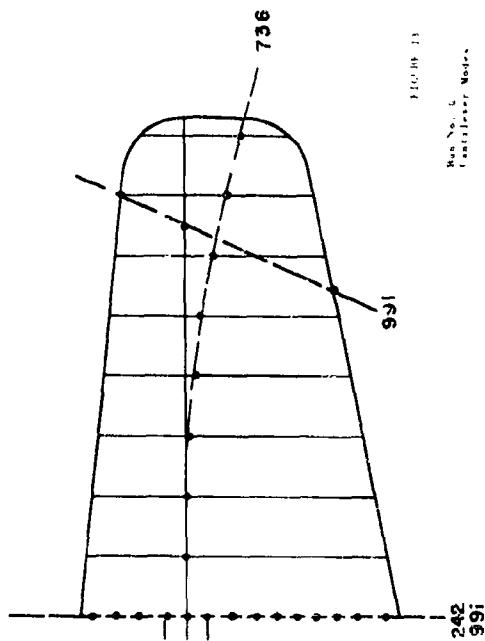
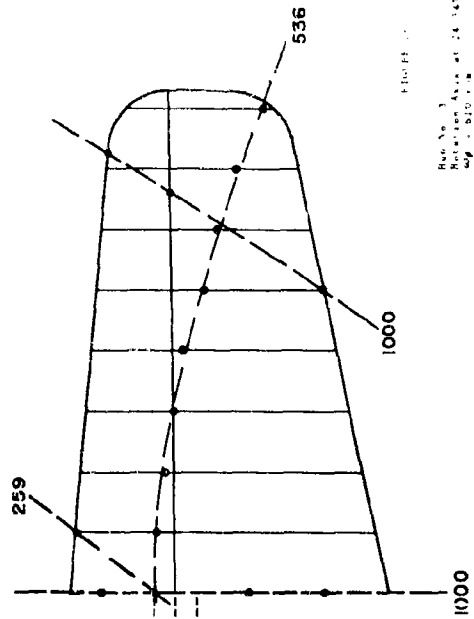
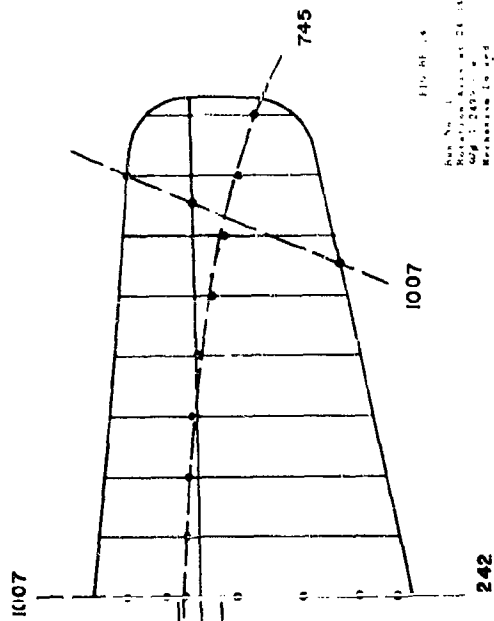
VI. CONCLUDING REMARKS

The results of a series of subsonic wind tunnel tests on a flutter model of an unswept all-movable horizontal tail have been presented. The chief facts learned from this investigation are the following:

1. Flexibility in the actuating mechanism of an unswept all-movable tail results in a serious lowering of the critical flutter speed.
2. For a given stiffness of the stabilizer actuating system the position of the axis of rotation has no appreciable effect on the flutter speed.
3. Very small amounts of free play in the actuating mechanism cause a significant decrease in the critical flutter speed without free play. When the free play exceeds $1/2^\circ$, the critical speed is greatly lowered although the flutter oscillations are relatively mild. This behavior was determined for only one location of the axis and one value of rotational restraint.

CONFIDENTIAL

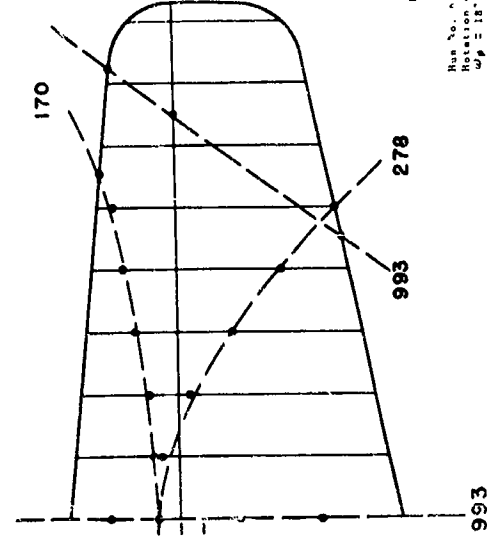
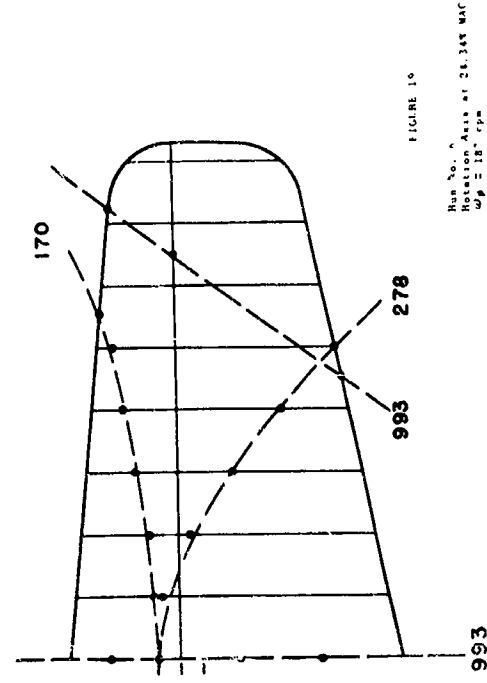
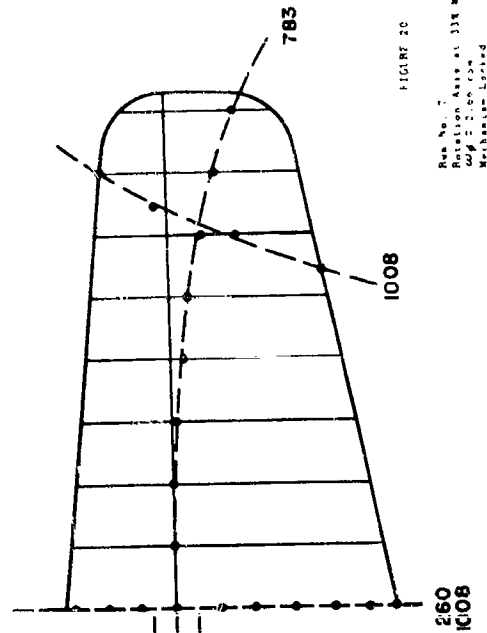
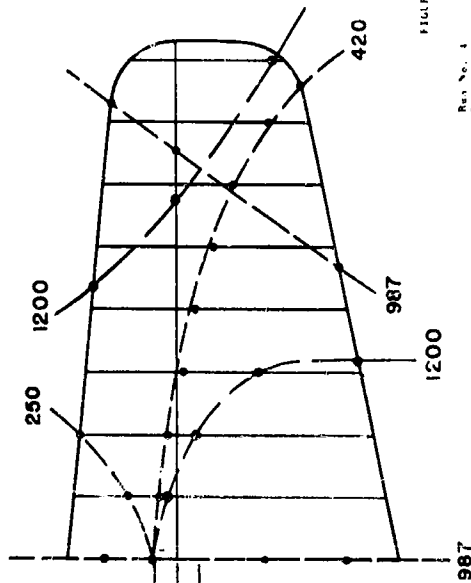
CONFIDENTIAL



Zero Airspeed Vibration Mode Lines and Frequencies

CONFIDENTIAL

CONFIDENTIAL



Zero Airspeed Vibration Node Lines and Frequencies (Continued)

CONFIDENTIAL

CONFIDENTIAL

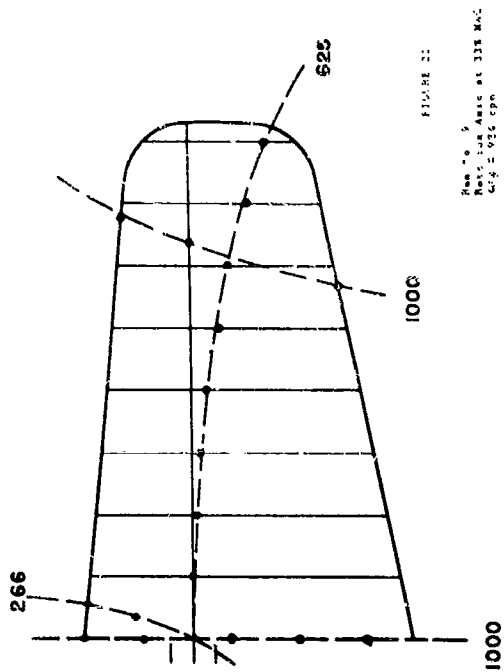


FIGURE 20
Run No. 5
Rotation Axis at 33% MAC
 $\omega_p = 926$ rpm

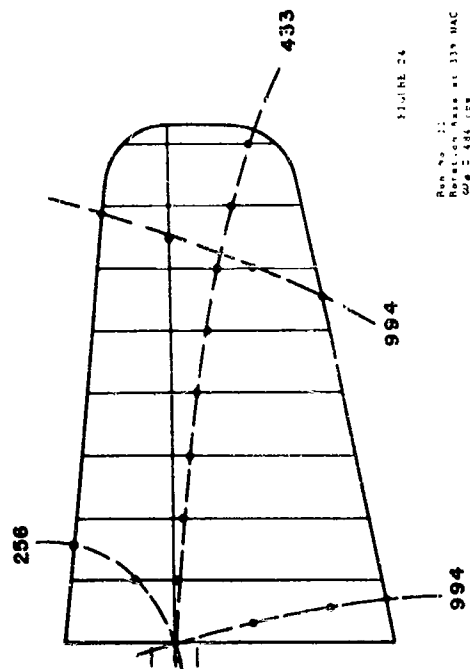


FIGURE 21
Run No. 21
Rotation Axis at 33% MAC
 $\omega_p = 484$ rpm

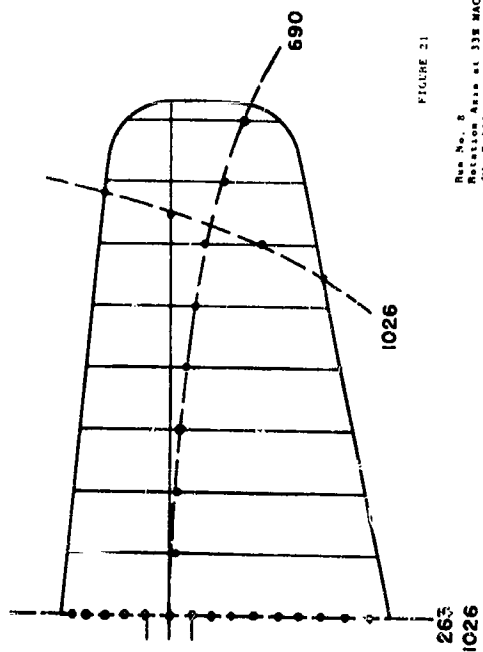


FIGURE 22
Run No. 8
Rotation Axis at 33% MAC
 $\omega_p = 1128$

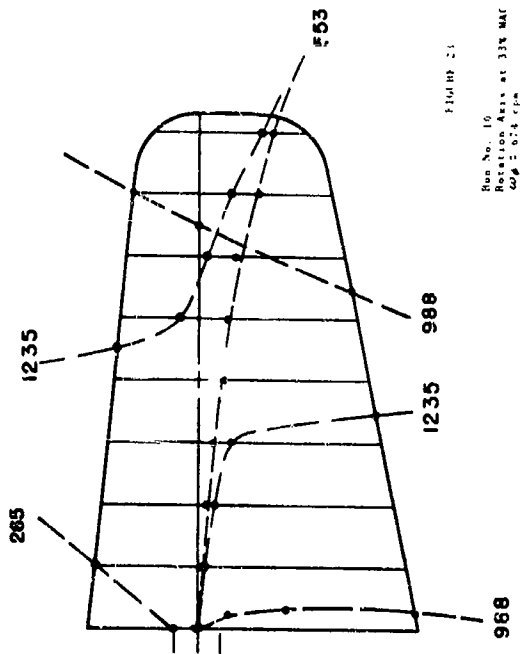
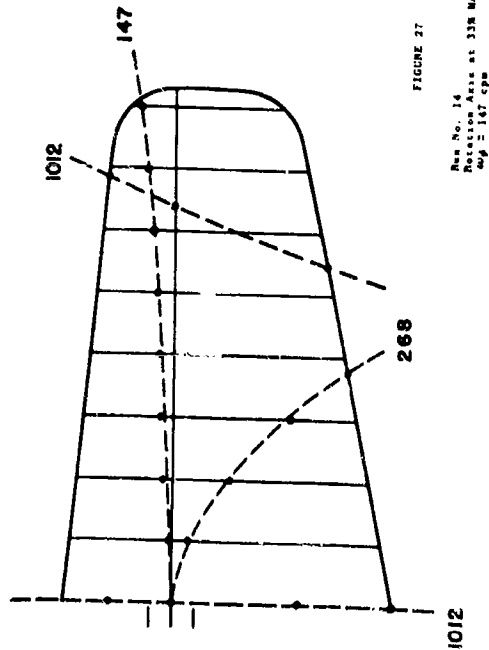
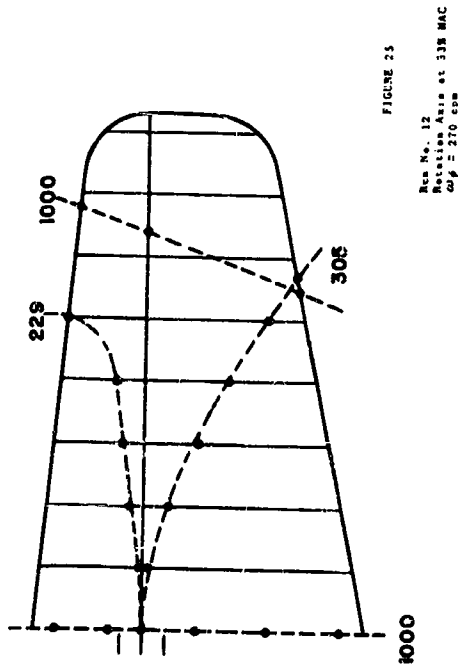
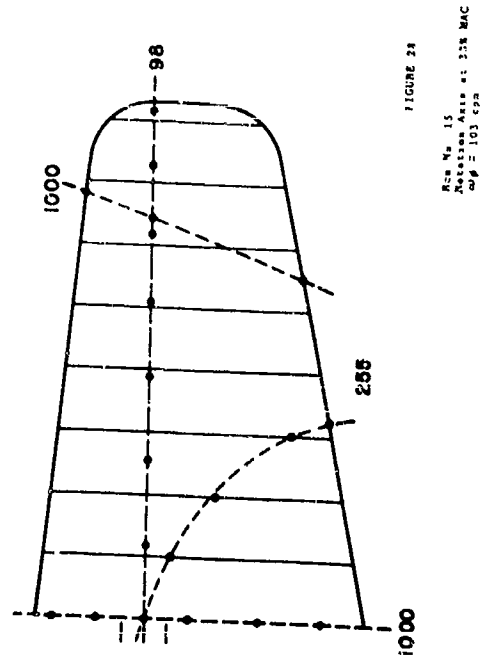
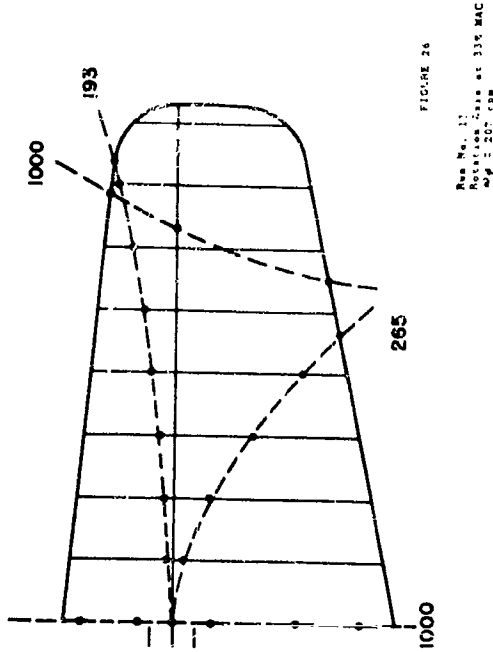


FIGURE 23
Run No. 10
Rotation Axis at 33% MAC
 $\omega_p = 674$ rpm

Zero Airspeed Vibration Node Lines and Frequencies (Continued)

CONFIDENTIAL

CONFIDENTIAL



Zero Airspeed Vibration Node Lines and Frequencies (Continued)

WADC TR 54-53

25

CONFIDENTIAL

CONFIDENTIAL

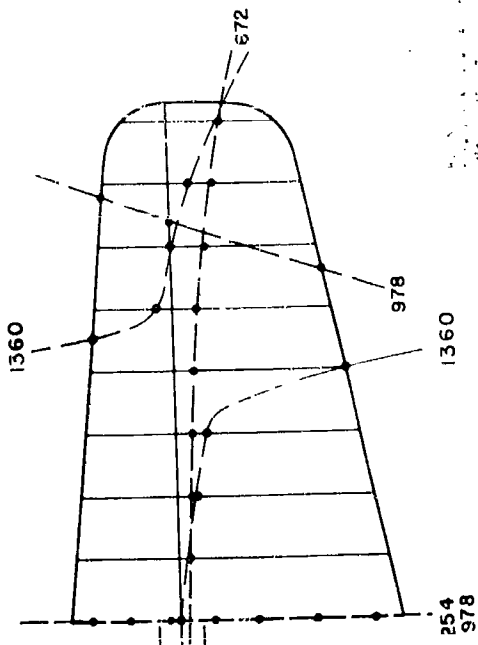


FIGURE 1
RELATIVE AIRSPEED - 0.500 MA
WING 100% DEFLECTED

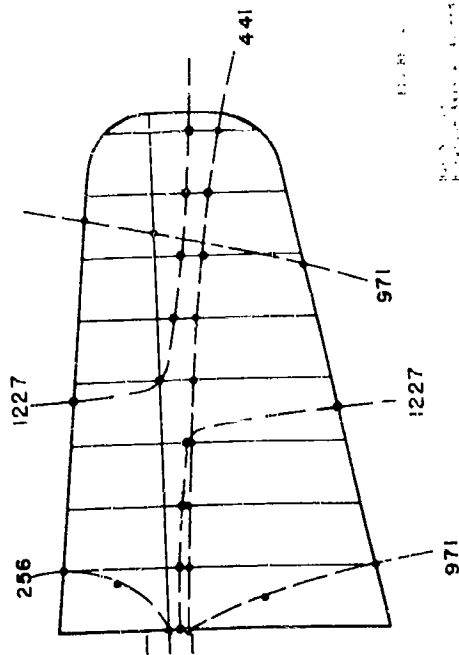


FIGURE 2
RELATIVE AIRSPEED - 0.500 MA
WING 100% DEFLECTED

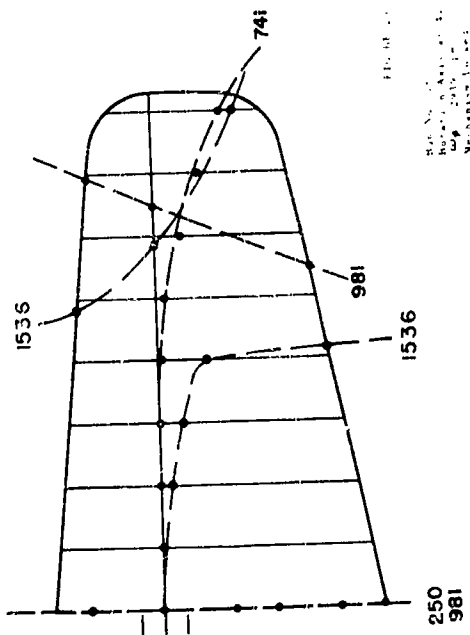


FIGURE 3
RELATIVE AIRSPEED - 0.500 MA
WING 100% DEFLECTED

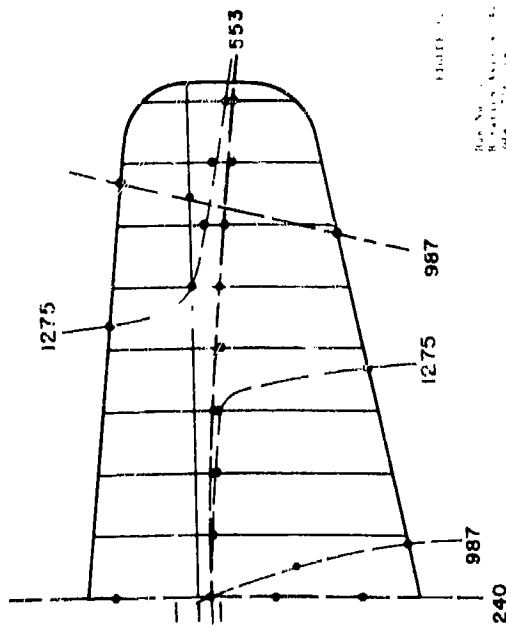


FIGURE 4
RELATIVE AIRSPEED - 0.500 MA
WING 100% DEFLECTED

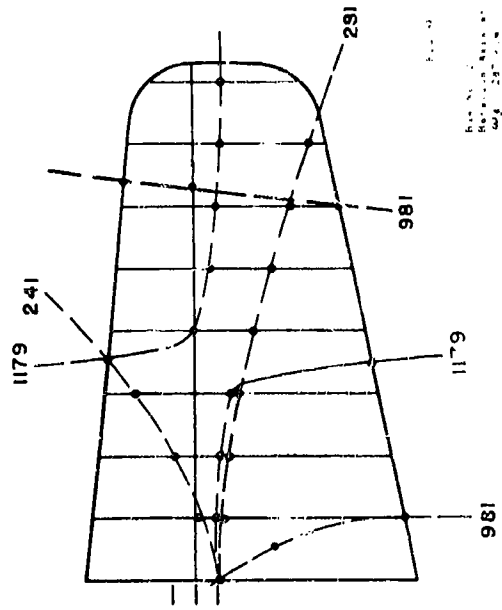
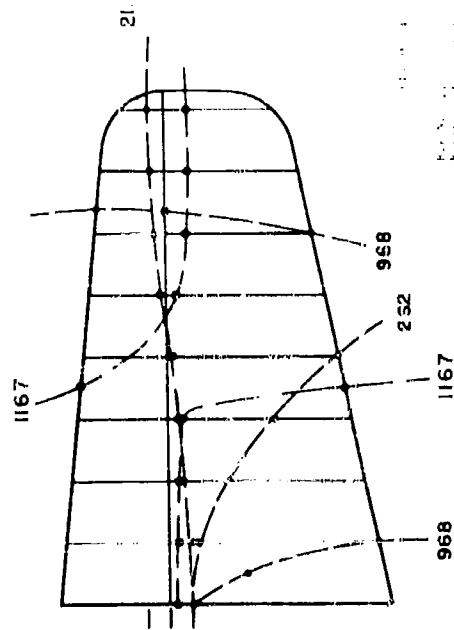
WADC TR 51-53

26

Zero Airspeed Vibration Spectra for Pre-Wing (Continued)

CONFIDENTIAL

CONFIDENTIAL



WALC 7K 9L-93

27

CONFIDENTIAL